

## Article

# Diurnal Characteristics of Heavy Precipitation Events under Different Synoptic Circulation Patterns in the Middle and Lower Reaches of the Yangtze River in Summer

Haixia Qi <sup>1,2</sup> , Chunze Lin <sup>1,\*</sup>, Tao Peng <sup>1,2,\*</sup>, Xiefei Zhi <sup>3</sup>, Chunguang Cui <sup>1</sup>, Wen Chen <sup>4</sup>, Zhiyuan Yin <sup>1</sup>, Tiejuan Shen <sup>1</sup> and Yiheng Xiang <sup>1</sup>

<sup>1</sup> China Meteorological Administration Basin Heavy Rainfall Key Laboratory, Hubei Key Laboratory for Heavy Rain Monitoring and Warning Research, Institute of Heavy Rain, China Meteorological Administration, Wuhan 430205, China; qxyxl@163.com (H.Q.); cgcui@whihr.com.cn (C.C.); yinzy@whihr.com.cn (Z.Y.); ssttyy@whihr.com.cn (T.S.); yiheng@whihr.com.cn (Y.X.)

<sup>2</sup> Three Gorges National Climatological Observatory, Yichang 415323, China

<sup>3</sup> Key Laboratory of Meteorological Disasters, Collaborative Innovation Centre on Forecast and Evaluation of Meteorological Disasters, Ministry of Education, Nanjing University of Information Science and Technology, Nanjing 211544, China; zhi@nuist.edu.cn

<sup>4</sup> Department of Atmospheric and Oceanic Science, University of Maryland, College Park, MD 20742, USA; chenwen\_602@126.com

\* Correspondence: linchunze@whihr.com.cn (C.L.); pt\_mail@whihr.com.cn (T.P.)

**Abstract:** Aiming at the rainstorm days ( $\geq 50$  mm/d) in the middle and lower reaches of the Yangtze River during 2010–2020, the obliquely rotated principal component in T-mode (PCT) method is used to classify the daily mean 850 hPa geopotential height, including Type 1 (vortex/shear line), Type 2 (frontal surface), Type 3 (warm shear line), Type 4 (warm inverse trough line), Type 5 (typhoon-westerly trough), and Type 6 (easterly wave). We studied the weather system configurations of different synoptic circulation patterns, their long-term trends, and their impacts on diurnal variations of heavy precipitation and drew the following conclusions: Type 1, Type 2, or Type 3 shows balanced double-peak frequencies of the start time of heavy precipitation during 06:00–08:00 BT and around 17:00 BT, respectively. For Type 1, dynamical lifting and thermal lifting play balanced roles, while for Type 2 and Type 3, dynamical lifting plays a key role. The number of rainstorm stations for Type 1 shows a slight increasing trend, while that for Type 2 or Type 3 shows a significant increasing trend. Type 4, Type 5, or Type 6 show a significant single peak frequency of the start time during 15:00–16:00. Type 5 and Type 6 are mainly affected by dynamical lifting along with favorable cape values, which can trigger rainstorms. The number of rainstorm stations for Type 4 or Type 6 shows a decreasing trend (that for Type 4 is more significant), while that for Type 5 shows a slightly increasing trend.

**Keywords:** PCT; synoptic circulation patterns; Bayesian model averaging; heavy rainfall



**Citation:** Qi, H.; Lin, C.; Peng, T.; Zhi, X.; Cui, C.; Chen, W.; Yin, Z.; Shen, T.; Xiang, Y. Diurnal Characteristics of Heavy Precipitation Events under Different Synoptic Circulation Patterns in the Middle and Lower Reaches of the Yangtze River in Summer. *Atmosphere* **2023**, *14*, 1320. <https://doi.org/10.3390/atmos14081320>

Academic Editor: Tomeu Rigo

Received: 25 May 2023

Revised: 12 July 2023

Accepted: 28 July 2023

Published: 21 August 2023



**Copyright:** © 2023 by the authors. Licensee MDPI, Basel, Switzerland. This article is an open access article distributed under the terms and conditions of the Creative Commons Attribution (CC BY) license (<https://creativecommons.org/licenses/by/4.0/>).

## 1. Introduction

Synoptic-scale systems that most directly cause rainstorms in the middle and lower reaches of the Yangtze River (MLRYR) are diverse, and the rainstorms caused by different synoptic systems are distributed in different spatial patterns. Therefore, it is necessary to classify synoptic systems using subjective or objective methods based on the large-scale circulation background where the rainstorms occur and analyze the impacts of different synoptic circulation patterns on the spatial and temporal distribution and diurnal variations of rainstorms, as well as the interactions and driving mechanisms between upper and lower systems [1–3]. Rao et al. [1] showed that over the Pearl River Delta, South China, due to the strong windward mechanical lifting and moisture transport, the number of convection occurrences was characterized by a dominant diurnal afternoon peak in the high-wind-speed days. Despite the weak orographic mechanical lifting on low-wind-speed days, the

number of convection occurrences had two comparable peaks in the afternoon and early morning. The nighttime peak is attributed to the nocturnal acceleration of the low-level southwesterly wind associated with the inertial oscillation and the corresponding enhanced windward lifting effects.

Diurnal variation is the basic change period of Earth's climate system, with solar radiation as the main driving force. Studying the diurnal variation in precipitation is very helpful to understand the physical laws of the evolution of regional weather and climate and the mechanism of precipitation formation. On this basis, conducting research on the uncertainty of numerical model results can provide a clear entry point for the development and improvement of numerical models [4–6]. He et al. [7] found that 62.2% of daytime mesoscale convective systems (MCSs) and 67.7% of nocturnal MCSs occurred in meridional atmospheric circulations, which were associated with the Northwest Pacific subtropical high (WNPSH). In addition, the number of MCSs decreased significantly from 2008 to 2010 over East China, which might be attributed to changes in the location of WNPSH, the trough to the west, and the low-level jets between the two systems.

Studies have shown that the diurnal precipitation peak falls into three categories: Single afternoon peak, continuous afternoon peak, and nocturnal peak. The continuous afternoon peak combines rainfall from two systems, one locally generated and one propagated [8–11]. The diurnal variation of land precipitation usually peaks in the afternoon due to the atmospheric response to radiative heating. In addition, the midnight-to-early-morning peak also exists in some areas influenced by complex topography and the land–sea distribution [12–15]. Li et al. [16] stated that the early morning rainfall in the southern periphery of the Tianshan Mountains is triggered locally in the southern basin. Both the late afternoon peak in the mountains and the night peak in the northern periphery are affected by mountain-originated rainfall events. These rainfall events tend to occur in mountain areas in the afternoon, and some of them move northward and lead to nocturnal rainfall in the northern basin.

Different levels of precipitation have different diurnal features, of which the diurnal variation of heavy precipitation is mainly divided into long-duration ( $\geq 6$  h) and short-duration ( $\leq 3$  h) heavy precipitation [17]. The long-duration heavy precipitation features stratiform-cloud rainfall with peaks occurring often from midnight to early morning, while the short-time severe convective precipitation has peaks mostly seen from afternoon to midnight [18–21]. Scientists have studied the mechanisms of diurnal variation in precipitation occurrence in various regions. Yu et al. [6] found that more than 60% of the total precipitation comes from persistent rainfall events ( $\geq 6$  h) through studying the daily precipitation in central-eastern China. The maximum hourly rainfall tends to occur in the early morning, while short-time severe rainfall events (1–3 h) usually reach their peaks in the late afternoon. Yu et al. [17] further proposed the asymmetry of the precipitation process, i.e., that hourly rainfall intensity grows to its peak value very fast from the beginning but decreases slowly from the peak to the end. Such asymmetry is more clearly seen in short-duration severe precipitation with complex topography. Chen et al. [22], pointed out that long-duration severe rainfall accounts for most of the rainfall along the Yangtze River, but it usually does not start in the afternoon in the upper reaches.

Previous studies have also simulated the diurnal variation of precipitation with regional numerical models and analyzed satellite radar and various common fusion data, concluding that the main source of the diurnal peak of heavy precipitation is MCS [23–28]. Nesbitt and Zipser [29] studied two different precipitation peaks in land areas using TRMM, pointing out that MCS activity is strongest in the evening, but precipitation peaks appear in the late night to early morning, and the non-mesoscale convective precipitation usually reaches its peak in the afternoon. The above-mentioned diurnal variation of precipitation is the analysis of actual rainfalls according to observation and simulation results, but from the synoptic-scale system that causes precipitation, especially heavy precipitation in China, the weather system can be roughly divided into 5 types: (1) Low-level vortices, such as the southwest vortex generated in Sichuan, the northwest vortex on the Qinghai–Tibet

Plateau, and the Ta-pieh vortex near the Ta-pieh Mountain; (2) low-level shear lines, near which there often exists the convergence of winds, causing vertical upward motion, which releases unstable energy and brings heavy rainfall; (3) frontal surface, which mainly refers to the cold front, warm front, and Meiyu front in East Asia; (4) tropical cyclone (TC); and (5) the peripheral circulation of subtropical high [30–37]. However, there are relatively few articles on how each synoptic system affects the diurnal variation of precipitation.

The spatial distribution of diurnal variability tends to be inhomogeneous because of various physical processes. The MLRYR basin (108° E–122° E, 24.5° N–33.5° N) (Figure 1) is oriented east-west. The distance of each place in the basin from the eastern coastal areas differs greatly, and the effect of the weather system on torrential rainfall is also different. The topography in the basin is complex, with inland mountains in the area west of 112° E, plains in 112° E–114° E, mountains and hills in 114° E–116° E, and again plains in the lower Yangtze River basin. In general, mountains and plains are dotted alternately in the basin, with the Yangtze River running through. The basins are important agricultural and densely populated areas in China, but they are also areas with frequent heavy rainfall and floods. Due to the impact of climate change and human activities, heavy precipitation and floods have frequently occurred in the middle and lower reaches of the Yangtze River in recent years, posing serious hazards in agricultural losses, urban floods, mountain landslides, soil erosion, and other aspects, so it is a suitable area for studying the variation characteristics of heavy and extreme precipitation.

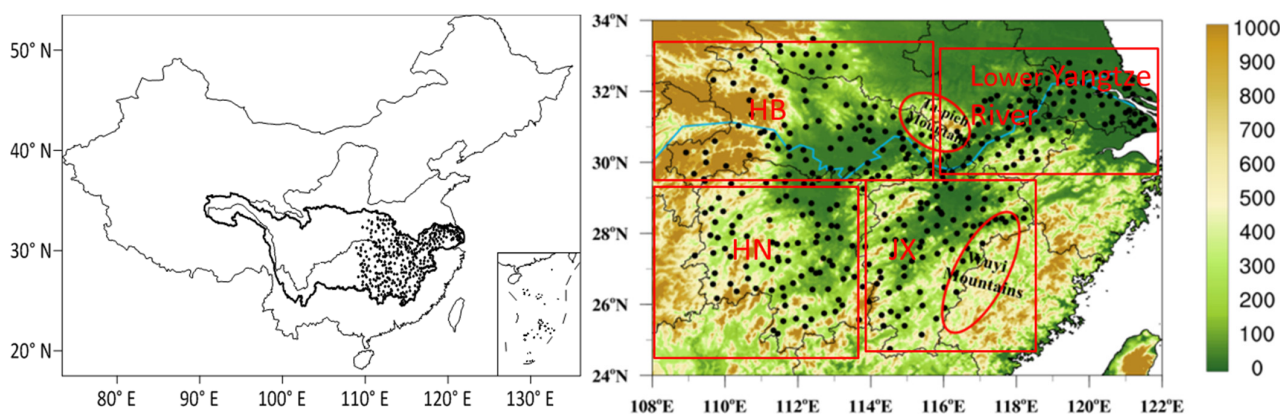


**Figure 1.** The spatial distribution of 367 rain gauge stations (black dots) in the middle and lower Yangtze River regions used in this paper. Mainly including four regions: Hunan Province (HN), Hubei Province (HB), Jiangxi Province (JX), and the lower reaches of the Yangtze River. Two important mountains are labeled as follows: Ta-pieh Mountains and Wuyi Mountains (red solid line). Shadings represent surface elevation (Unit: km).

The present study is in the MLRYR basin. And here, we aim to answer the following questions: What are the impacts of different synoptic circulation patterns on the diurnal variation features of heavy precipitation in summer in the MLRYR? What are the configurations of their upper and lower synoptic systems? In addition, what are their long-term trends?

The paper is divided into the following sections: Section 2 briefly describes the data and methods. Section 3 describes the impacts of different synoptic circulation patterns on the diurnal variation features of heavy precipitation over the MLRYR basin. Section 4 describes the configurations of their upper and lower synoptic systems and their driving mechanisms for heavy precipitation. In Section 5, long-term trends under six synoptic circulation patterns are given, and finally, Section 6 is the conclusion and discussion.

## 2. Data and Methods

The datasets of hourly rainfall at 367 stations covering the MLRYR region for the period June–August from 2010 to 2020 are used in this study. The sample numbers for each

hourly data are 1012 h. These datasets were obtained from the national climatic reference network, with quality controlled by the National Meteorological Information Centre of the China Meteorological Administration (NMIC/CMA). A day with precipitation  $\geq 50$  mm/d at more than three adjacent stations (the distance between stations is not more than 100 km) is called a rainstorm day in the study region [38]. A total of 487 rainstorm days were selected from the June–August precipitation data in 2010–2020.

In the past, researchers often used subjective experience and daily synoptic charts to classify the rainstorm days, while the obliquely rotated principal component in T-mode (PCT) method can greatly improve the efficiency of studying the hourly precipitation characteristics in long-time series [39–41]. We briefly summarize the PCT approach to the classification of circulation patterns. PCT consists of expressing a data matrix  $Z = (z_{ij})$ ,  $i = 1, \dots, N$  indexing observations (individuals), and  $j = 1, \dots, n$ , indexing times, in the form of a product  $Z = FA^T$ . Here,  $F$  is the matrix of principal component (PC) scores (amplitudes), and  $A$  is the matrix of PC loadings. The loadings are the eigenvectors of the data correlation (or covariance). All PCs are sorted according to the corresponding eigenvalues. The larger the eigenvalues, the greater the contribution to the original data. The PC scores of each subset are projected onto the remaining data through the oblique rotation of the gradient projection algorithm, and the type with the highest daily load is selected as the classification result for this day. The PCT method, which was developed in the project ‘Coordination and Application of Weather Classification Methods in Europe’ as a software package of `cost733class-1.2_RC_revision8` [40,41], can be downloaded from the official website: <https://projects.met.no/cost733/> (accessed on 6 May 2023).

For the MLRYR (23°–40° N, 107°–132° E), the 850 hPa geopotential height field can not only reflect the synoptic system of severe precipitation but also connect the synoptic systems in the upper and lower atmosphere. When performing weather classification of heavy rainfall days, we use the 850 hPa daily mean height field from the ERA5 reanalysis data released by the European Centre for Medium-Range Weather Forecasts [42], from June to August 2010–2020, as a physical quantity field (the average value of the four times 08:00, 14:00, 20:00, and 02:00 BT (Beijing time)), covering a range of 106–130° E, 23–40° N, with a temporal resolution of 1 h and a spatial resolution of  $0.25^\circ \times 0.25^\circ$ . The number of software classifications is six circulation types. After the processing of the classification software, the files of the geopotential height fields of six circulation types and the files of the dates of the 487 rainstorm days corresponding to the circulation types are finally generated.

This paper focuses on the classification of the characteristics of heavy precipitation events under different synoptic circulation patterns. The following conditions need to be satisfied for short- and long-duration heavy precipitation events: (1) Short-duration heavy precipitation is defined as the precipitation  $\geq 20$  mm/h at any time within 3 h or the total precipitation  $\geq 30$  mm for consecutive 3 h and  $\geq 5$  mm in 1 h at a single station. (2) Medium-to-long duration heavy precipitation refers to total precipitation  $\geq 30$  mm and precipitation  $\geq 5$  mm in 1 h in continuous 4–5 h at a single station. (3) Long-duration heavy precipitation refers to total precipitation  $\geq 30$  mm and precipitation  $\geq 5$  mm in 1 h in continuous 6 h or longer time at a single station. (4) After the cases are selected, the start time of heavy precipitation is set as the first time when the precipitation at a single station is  $\geq 5$  mm and the precipitation of the previous time is  $< 0.1$  mm; the end time is set as the time when the single-station precipitation is  $< 0.1$  mm during the duration of the rainstorm.

### 3. Diurnal Variation Features of Heavy Precipitation under Six Synoptic Circulation Types

#### 3.1. Objective Circulation Weather Classification of Rainstorm Days

Based on the PCT classification method on 850 hPa height and combined with the average 700 hPa wind, surface pressure, and 850 hPa temperature of all individual cases of six types, rainstorm days in the MLRYR are generated according to the principles of weather science. They combine the synoptic-scale and mesoscale atmospheric conditions affecting heavy precipitation. These circulation types are Type 1: Vortex/shear line (Figure 2a);

Type 2: frontal surface (Figure 2b); Type 3: warm shear line (Figure 2c); Type 4: Warm inverse trough line (Figure 2d); Type 5: Typhoon-westerly trough (Figure 2e); and Type 6: Easterly wave (Figure 2f). The definitions of Types 2–4 will be mainly explained. Type 2 frontal surface is the interface of two air masses (cold air and warm air) with different physical properties, such as temperature and humidity. This is mainly based on the analysis of dense zones of sea level pressure and 850 hPa temperature fields. Type 3 warm shear line refers to the shear line composed of southeast and southwest winds or easterly and southerly winds, in which the southwest or southerly wind is dominant. Pushing the shear line from south to north, it is similar in nature to a warm front. Type 4 warm inverse trough line is a trough of low pressure with an opening to the south or southwest in the middle and low latitudes.

The corresponding geopotential heights, wind vectors, or temperature, and the occurrence probability of rainstorm ( $POP \geq 50 \text{ mm/d}$ ) for each synoptic pattern are shown in Figure 2. POP at a station is defined as the ratio of total rainstorm occurrences under a given synoptic pattern to the total occurrences of the specific synoptic pattern. A higher occurrence probability implies that the rainstorm is more likely to happen there under such a pattern. With the monsoon and rain band moving northward, the major circulation patterns causing rainstorms over the MLRYR basin in the summer have also changed.

The number and frequency of rainstorm days under the first three circulation patterns (Type 1, Type 2, and Type 3) contributed by southwesterly monsoon flows are relatively high, reaching 359 days within 487 rainstorm days, accounting for about 73.7%. These three types are the primary rainstorm weather types in MLRYR. The occurrence frequencies for the other three patterns (Type 4, Type 5, and Type 6) are much smaller with the easterly flow. The early summer rainstorms are mainly dominated by the Type 3 warm shear line (33 days, 6.8%, Figure 2c), and heavy precipitation events mainly occur in the HuaNan and Jiangxi provinces to the south of the Yangtze River. During the Meiyu season, the low vortex prevails, spreading along the Yangtze River. The most frequent occurrences of Type 1 are 189 days, 38.8% (Figure 2a), with the maximum occurrence probability concentrated in the region about 200 km north-south along the Yangtze River. Type 2 rainstorms account for around 28% of total rainstorms (Figure 2b), have the typical characteristics of the Meiyu front under low-level winds with southwesterly winds, and occur in the lower Yangtze River and Northeastern Jiangxi with a high occurrence probability (more than 8%). After the Meiyu period comes to an end, easterly waves and typhoon activities frequently occur in the easterly wind area to the south of the subtropical high ridge, which have become the main weather types causing rainstorms over the MLRYR basin. Type 4 warm inverse-trough type (Figure 2d) contributes about 17% (82 days) of total rainstorms and is characterized by prevailing southeasterly winds, under which occurrence probability concentrates in the eastern part of the basin, with fewer rainstorm days in areas to the west of Hubei and Jiangxi. There are 24 days of heavy precipitation under Type 5 (typhoon-westerly trough type, Figure 2e), accounting for 4.9% of rainstorm days. The heavy precipitation occurrence probability concentrates along the lower Yangtze River, Hunan, and Southern Jiangxi regions. The easterly wave Type 6 (Figure 2f) occurs least frequently, taking up only 4.5% of the rainstorm days. The affected range is the smallest, and the rain-falling areas are scattered, mostly showing the characteristics of localized rainfall.

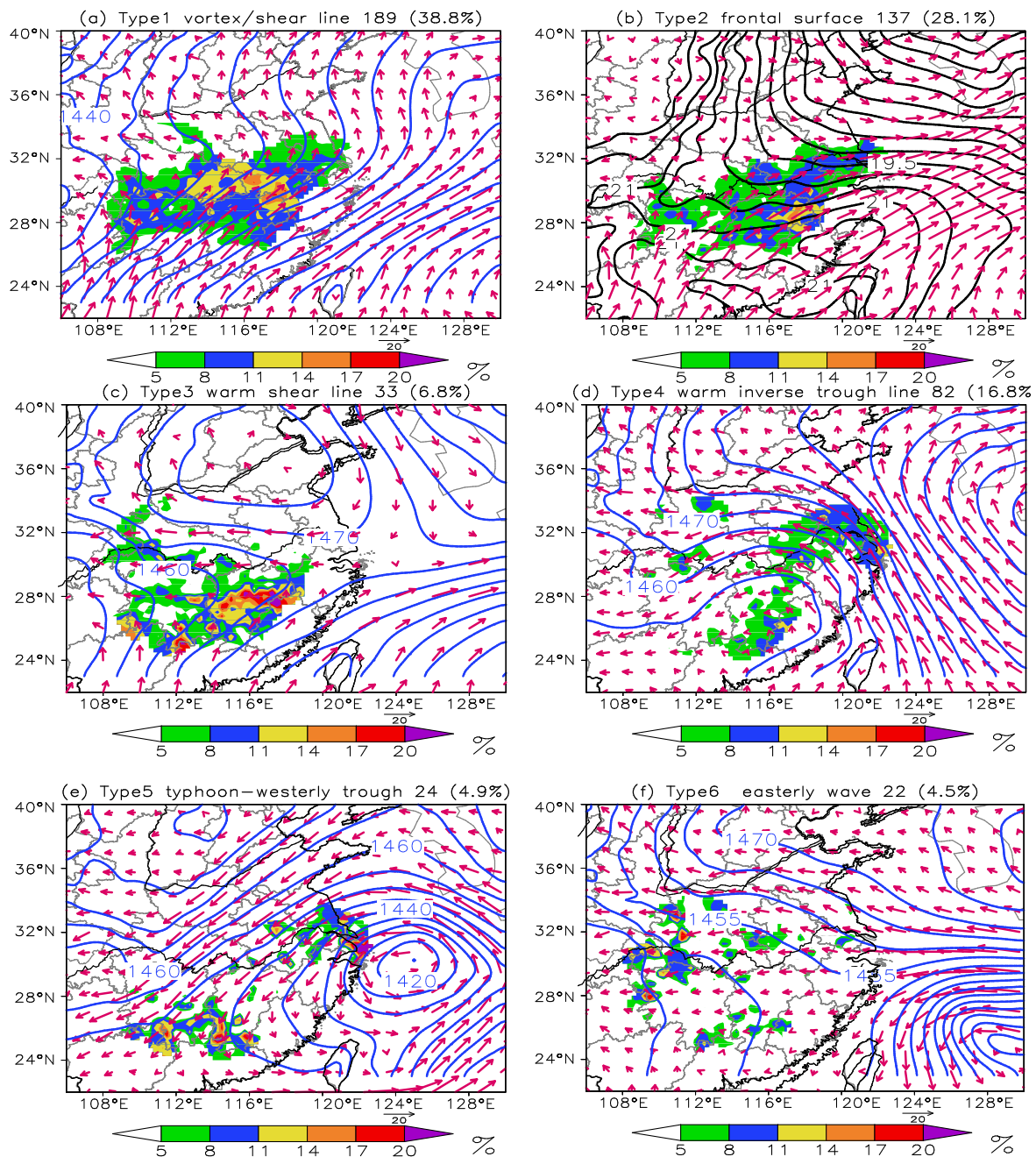


**Figure 2.** Six types of synoptic circulation patterns (purple curve) generated by the obliquely rotated Principal Component in T-mode (PCT) method based on the 850 hPa geopotential height field in the middle and lower reaches of Yangtze River. Shaded values are the occurrence probability of rainstorm days ( $\geq 50$  mm/d) under each synoptic circulation pattern. (Type 1: Vortex/shear line (a), Type 2: Frontal surface (b), Type 3: Warm shear line (c), Type 4: Warm inverse trough line (d), Type 5: Typhoon-westerly trough (e) and Type 6: Easterly wave (f)). (The synoptic circulation patterns below are the same as those given here. The blue curve represents the height, unit: gpm. The black curve represents the temperature at 850 hpa, unit:  $^{\circ}$ C, the meaning of the curve is the same below).

In order to study the weather systems under each pattern and the matching relationship between heavy precipitation areas, typical cases under each weather type were selected for research. Select for analysis. Figure 3a1–a3 shows the weather system configuration diagram at 08:00 on 18 July 2020 (Type 1: Vortex/shear line). At 500 hPa, there is a significant

eastward movement of the trough, while at 850 hPa, the southwest vortex trends northeast to southwest. There is a stationary front on the ground near the Yangtze River, and heavy precipitation mainly occurs near the weather system where the westerly jet and stationary front overlap in the front of the low trough and on the right side of the southwest vortex. Figure 3b1–b3 shows the configuration of the weather system on 16 June 2015 at 20:00 (Type 2: Frontal surface). There is a flat westerly airflow at 500 hPa. At 850 hPa, there is a clear temperature line and dense zone near 32° N, namely the front surface. On the ground, there is a significant thermal low system in the south of the front and a cold high-pressure system in the north. The south wind and north wind generated by the thermal low and cold high-pressure systems are opposite each other, and the heavy precipitation mainly occurs near 32° N. Figure 3c1–c3 shows the configuration of the weather system on 1 July 2014 at 08:00 (Type 3: Warm shear line). The western end of the Northwest Pacific subtropical high (WNPSH) extends to 104° E at 500 hPa. There is a strong southwest jet at 850 hPa, which forms a warm shear line with the northerly wind near 32° N. There are also weak, warm shear lines on the ground. The heavy precipitation mainly occurs near the warm shear line and at locations where the southwest jet is strong. Figure 3d1–d3 shows the configuration of the weather system on 19 June 2014 at 08:00 (Type 4: Warm inverse trough line). There is a shallow trough moving eastward above 500 hPa, and WNPSH is located at sea. The southwest jet stream at 850 hPa combines with the southwest wind flow of the low-pressure system, forming a warm inverse trough line at the top of the low-pressure system. The ground is also dominated by easterly airflow. Heavy precipitation mainly occurs near the trough line. Figure 3e1–e3 shows the weather system on 13 July 2013 at 08:00 (Type 5: Typhoon-westerly trough). The upper- and lower-level systems are dominated by the strong login typhoon system. The heavy rainfall in the middle and lower reaches of the Yangtze River mainly occurs near the typhoon. Figure 3f1–f3 shows the weather system on 8 June 2014 at 20:00 (Type 6: Easterly wave). There is a straight westerly airflow above 500 hPa. At 850 hPa, there is a tropical low-pressure system generated in the South China Sea region. The east-west airflow on the south side of WNPSH, combined with the easterly airflow on the north side of the tropical cyclone, moves from west to east. The ground system is not significant. Strong precipitation is mainly localized and dispersed, mainly occurring in areas with terrain barriers.

Almost half of the summer precipitation in the MLRYR comes from the Meiyu, which lasts for more than 20 days. Studying which weather type system produces heavy precipitation before, during, and after the Meiyu season can provide forecasters with scientific references. According to the statistics of the National Climate Center, CMA (Beijing, China), the average onset time of the 1951–2020 Meiyu in the MLRYR is 14 June, and the end time is 13 July. So, we take these two dates as nodes to calculate the occurrence frequency of the rainstorm under six synoptic circulation types before, during, and after the Meiyu season. The number of rainstorm days in each weather type in the three time periods (1–13 June, 12–14 June, and 13 July–31 August) is divided by the total number of heavy rain days in the time period. As seen from Figure 4, for Type 1 and Type 2, the rainstorm occurrence frequency before Meiyu is relatively small, both at around 5%, but during and after the Meiyu season, rainstorms are frequently seen, reaching 19% and 13%, respectively, so the highest frequency appears during the Meiyu season. The total number of rainstorm days during and after Meiyu amounts to 56% of the entire rainstorm days. As for Type 3, the frequencies of rainstorm before, during, and after Meiyu are similar, at a slightly higher rate. For Type 4, rainstorm usually occurs after the Meiyu season with a frequency of up to 78%, but only 3.6% before the Meiyu period. Type 5 has the highest occurrence frequency of rainstorm after Meiyu, accounting for about 63% of the total frequency, and the frequency is also relatively higher before Meiyu starts. The absolute large values of rainstorm occurrence frequency with Type 4 and Type 6 mainly occur after Meiyu, but less frequently before and during the Meiyu period; especially for Type 6, the frequency appears to be about 91% after Meiyu ends.

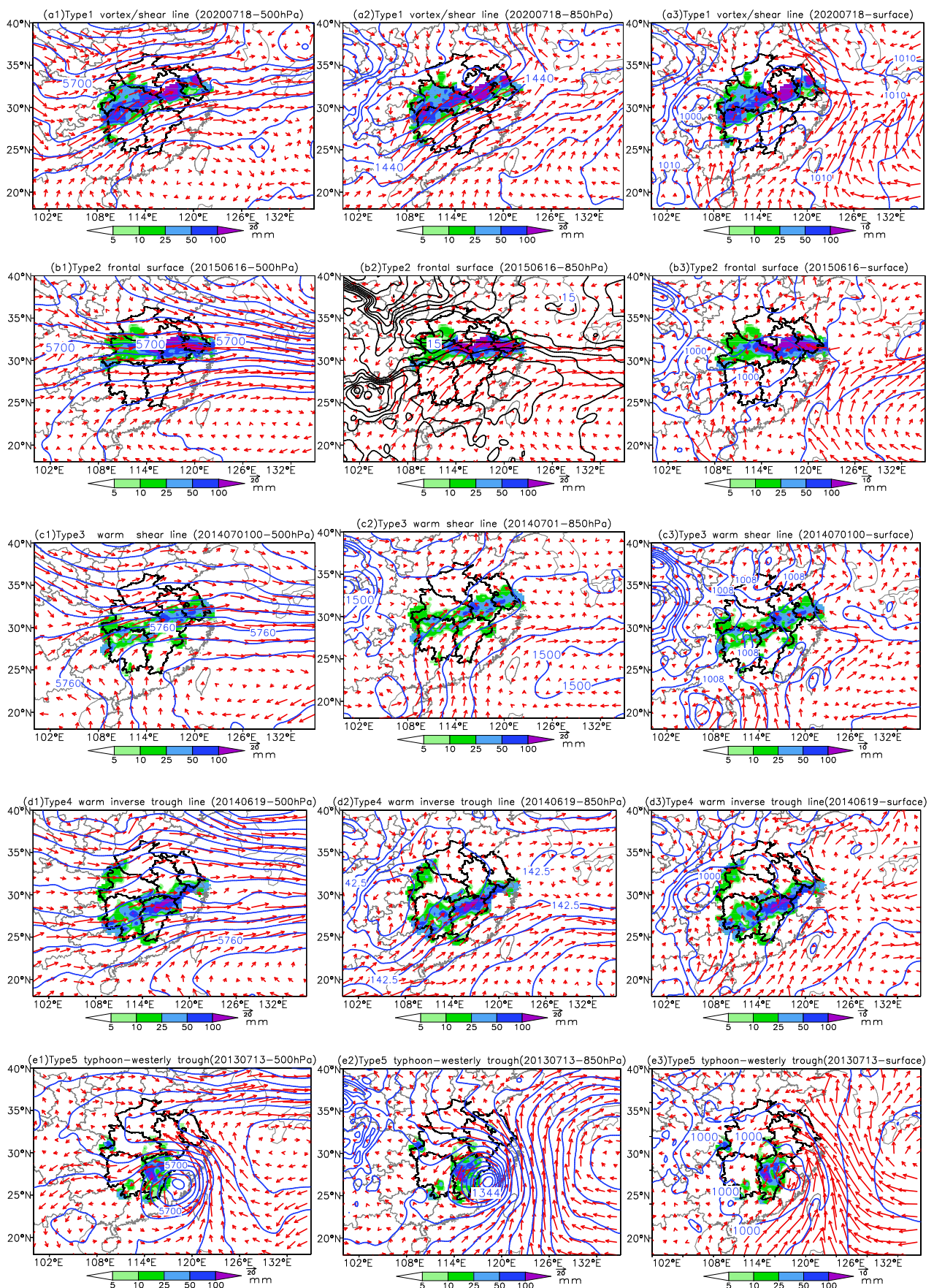
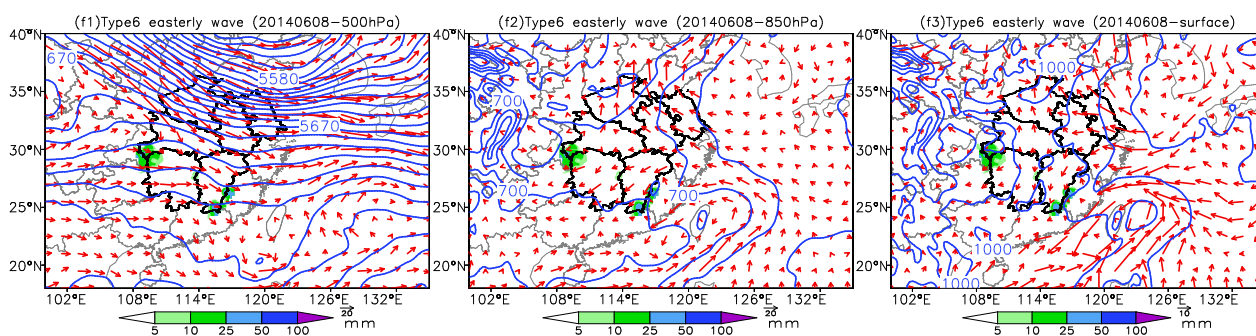
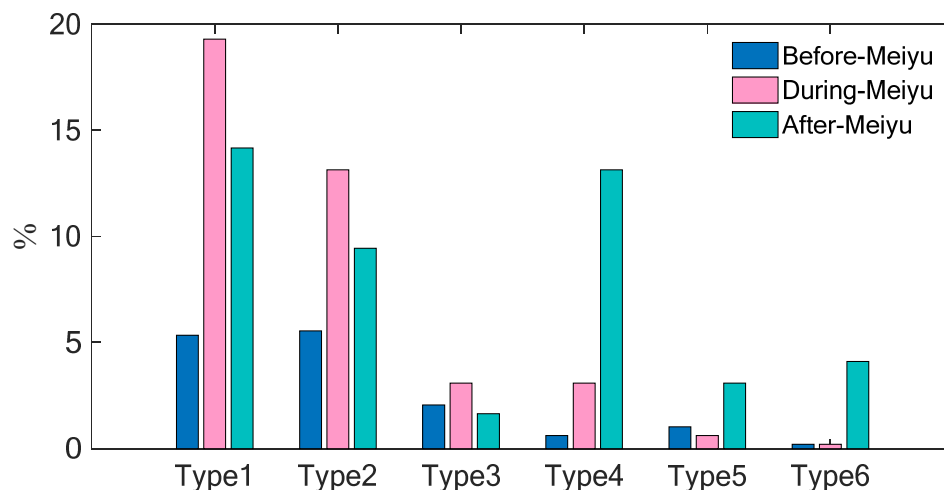


Figure 3. Cont.



**Figure 3.** The configuration weather system of typical cases of six weather circulation patterns. (a1,a2) are the height and wind fields at 500 hpa and 850 hpa, (a3) is the sea level pressure and 10m wind field respectively on 28 July 2020 under Type1 Vortex/shear line. Shaded values are the amount of precipitation under each pattern, unit: mm. (b1–b3), (c1–c3), (d1–d3), (e1–e3), (f1–f3) are the same as above, but for 16 Jun 2015 under Type2, 1 July 2014 under Type3, 19 Jun 2014 under Type4, 13 July 2013 under Type5, 8 Jun 2014 under Type6. The blue curve represents the height, unit: gpm. The black curve represents the temperature at 850 hpa, unit: °C).



**Figure 4.** Percentage of rainstorm days under the 6 synoptic circulation patterns (Type 1: Vortex/shear line, Type 2: Frontal surface, Type 3: Warm shear line, Type 4: Warm inverse-trough, Type 5: Tropical cyclone-westerly trough, and Type 6: Easterly wave) before Meiyu (1–13 June), during Meiyu (14 June–12 July), and after Meiyu (13 July–31 August). (Calculation method is dividing the rainstorm days under 6 types in each time period by the total 487 rainstorm days, and then multiplying by 100%).

In summary, in the MLRYR, Type 1 and Type 2 occur mainly during and after the Meiyu period, with the highest occurrence frequency during the Meiyu period, while Type 3 occurs relatively evenly in the three periods. Type 4 and Type 6 both have absolute large frequency values after the Meiyu season, during which their occurrence frequencies are as high as 78% and 91%, respectively. Type 5 has the highest frequency after the Meiyu season, accounting for 63% of the total frequency.

In order to understand the contribution of heavy precipitation to total precipitation under the six weather circulation patterns, it can be seen from Figure 5 that light rain accounts for the largest proportion of precipitation in all six types, reaching over 60%. The heavy rain (25 mm ≤ heavy rain < 50 mm) and rainstorm (≥50 mm) of types 2 and 4 account for more than other types, reaching over 15% and 10%, respectively, indicating that these two types are more prone to heavy precipitation in the middle and lower reaches of the Yangtze River. The rainstorm of Type 1 and Type 6 accounts for a relatively small proportion, about 6.8% and 6%, respectively, which indicates that the precipitation

generated by the rainstorm of these two types in this area is relatively small compared with the other magnitudes of precipitation.

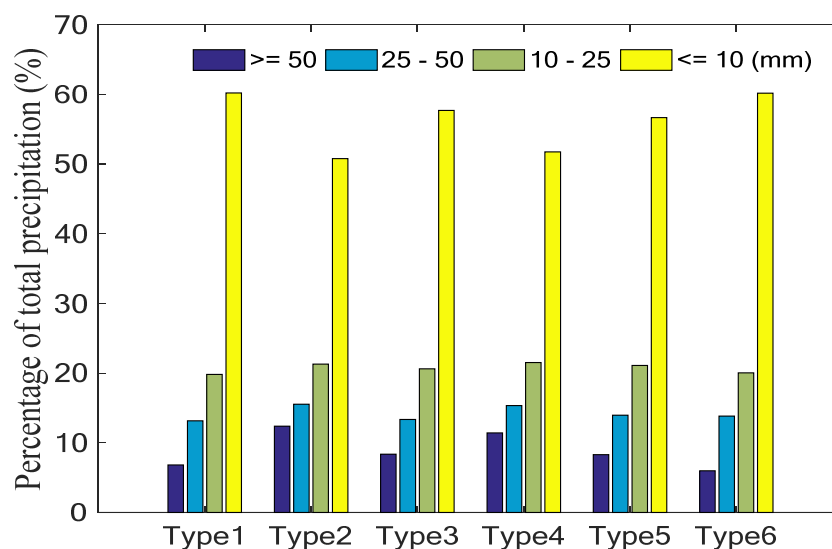


**Figure 5.** The percentage of different magnitude precipitation generated under six weather circulation patterns to their respective total precipitation (unit: %).

### 3.2. Differences in Starting Time and Duration of Heavy Precipitation

Previous studies have pointed out that, in addition to solar radiation, the diurnal variation of precipitation is often caused by uneven diabatic heating due to differences in terrain and landform between different areas, such as mountains and plains, land and sea [17,20,43]. Yu et al. [6] found that the persistence of precipitation is a key factor in separating the diurnal variation phases in central and eastern China: The peak values of long-duration precipitation occur mostly at night and in the early morning, while the maxima of short-duration precipitation occur mostly in the afternoon or evening. The short-duration precipitation peak in the afternoon can mostly be attributed to thermal instability caused by diurnal variations in solar radiative heating, while the peaks of long-duration precipitation in the early morning are mostly likely to be associated with large-scale circulations [43]. However, the impacts of different synoptic circulation patterns on the diurnal variation features of heavy precipitation were seldom studied in previous studies. The results of this paper will complement the previous findings. To study the differences in the diurnal variation of short-time and persistent heavy precipitation under the six synoptic circulations, we divide the severe precipitation into short-duration ( $\leq 3$  h) and long-duration ( $\geq 6$  h) rainstorms (Section 2: Data and Methods). According to the wind field directions of the dominant synoptic systems in the middle and lower layers, the six synoptic circulation patterns can be grouped into two types, one of which is dominated by the prevailing southwest monsoon (Types 1–3: southwest vortex/shear line, frontal surface, and warm shear line, Figure 6a–c). It reveals that all three types show double-peak patterns of the starting time peaks for short-duration and long-duration heavy precipitation. In contrast, the other type, dominated by the easterly flow (Type 4–6: Warm inverse trough line, cyclone-westerly trough, and easterly wave, Figure 6d–f), shows a significant single peak. It indicates that the peak of short-duration heavy precipitation is not only related to the afternoon solar radiation but also closely linked to the synoptic circulation pattern.

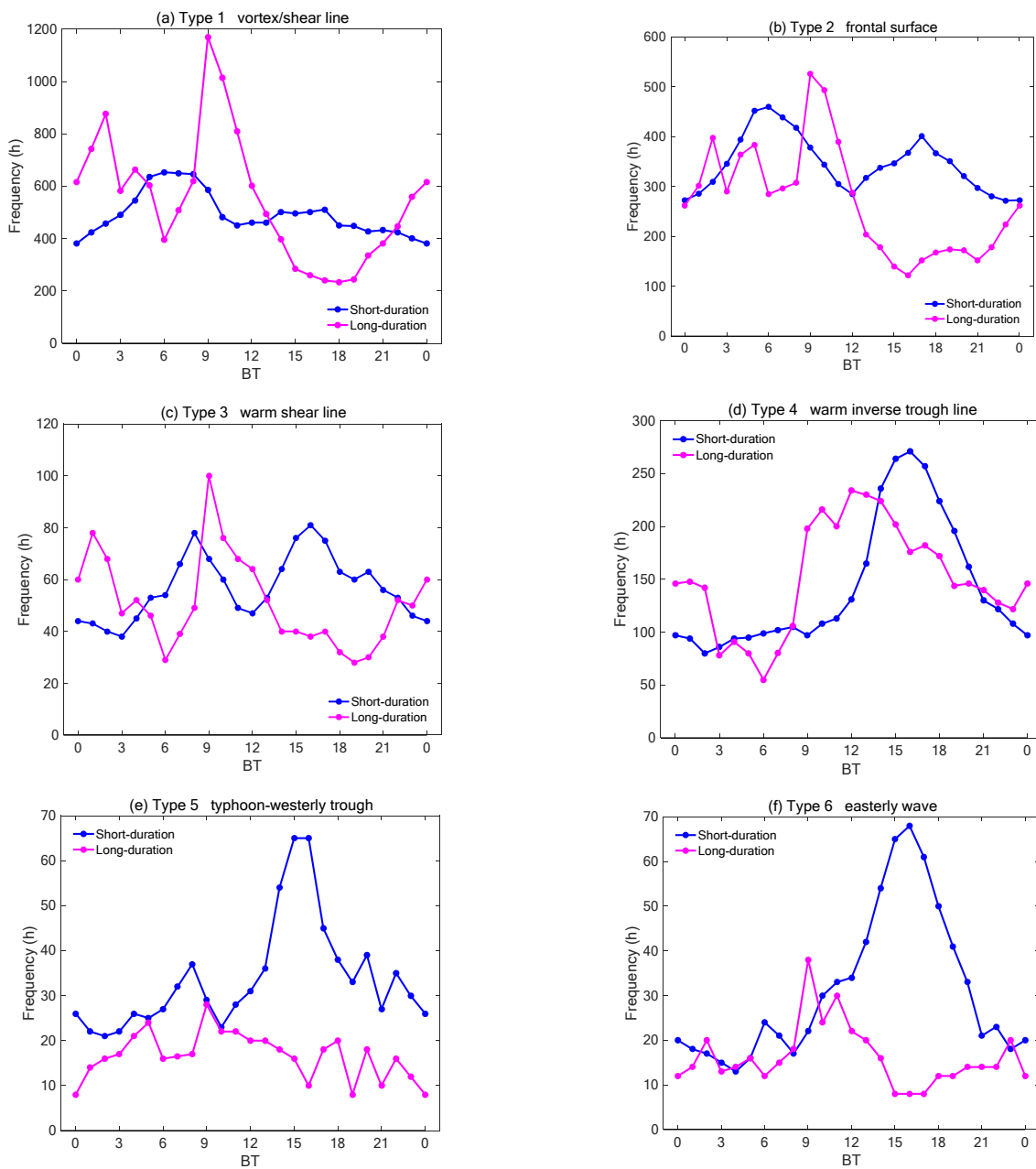


**Figure 6.** Hourly occurrence frequencies of the initial time of short-duration and long-duration rainstorms under the 6 synoptic circulation patterns. (The blue curve S-type refers to short-duration heavy precipitation  $\leq 3$  h, and the pink curve L-type refers to long-duration heavy precipitation  $\geq 6$  h). (a–f) figures represents six weather circulation patterns, as shown in Figure 2.

For Type 1, Type 2, and Type 3 (Figure 6a–c), from the perspective of the diurnal variation at the start time, it shows the relatively even double-peak patterns with equivalent frequencies of both peaks for short-duration heavy precipitation (blue line), and the maximum frequency of the start time appears during 06:00–08:00 BT and around 16:00–17:00 BT, while the lower frequencies are at approximately 00:00 BT and 12:00 BT. However, the peak patterns of long-duration heavy precipitation (pink line) show double peaks—A primary and secondary peak. The significant primary peak of the start time of severe precipitation often occurs around 09:00 BT, and the sub-peak time is observed at 01:00–02:00 BT in the night. Seen from the magnitude of frequency, the maximum frequency of long-duration Type 1 appears at 9:00 BT, recorded 1170 times, while the maximum frequency for short-duration heavy precipitation at 06:00 BT reaches 653 times, which is nearly half of the value

of 1170 times. This indicates that the heavy precipitation events caused by the low vortex or shear-line system are mostly persistent heavy precipitation events that start at night or in the morning (Figure 6a). The peak frequencies of short-duration and persistent heavy precipitation events of Type 2 and Type 3 are basically identical (Figure 6b,c), indicating that heavy precipitation events occurring under frontal and warm shear synoptic systems can be systematic persistent heavy precipitation events or short-duration convective heavy precipitation events.

Type 4, Type 5, and Type 6 (Figure 6d–f) show a significant single peak, with the peak frequency of the start time mainly concentrated during 15:00–16:00 BT for short-time heavy precipitation and 09:00–12:00 BT for the long-duration. The magnitude of the frequency of short-duration heavy precipitation is greater than that of long-duration heavy precipitation. Especially, the peak frequency of short-duration heavy precipitation for Type 5 and Type 6 is close to twice that of persistent heavy rainfall, indicating that the characteristics of short-duration heavy precipitation of these two synoptic circulations are more significant.

Specifically, for all the types, long-duration heavy precipitation tends to occur at 9:00 BT, which is a little later than the short-duration heavy precipitation at 6:00 BT. This may be due to the more stable long-duration precipitation system, which requires a greater accumulation of unstable energy.

### 3.3. Distribution Characteristics of Averaged Duration of Heavy Precipitation

Figure 7 gives the distribution characteristics of the average duration of severe precipitation under the six synoptic circulation patterns. The duration of rainstorm can be divided into short-duration ( $\leq 3$  h), medium-long duration (4–5 h), and long-duration ( $\geq 6$  h) heavy precipitation.

On the whole, the heavy precipitation process is mainly short-duration heavy precipitation (green dots), and the persistent heavy precipitation is the least in MLRYR. The spatial distribution of medium-long and long-duration heavy precipitation is closely related to the circulation pattern. In the following pages, we will only analyze the impacts of different synoptic circulation patterns on the distribution of medium-duration (blue dots) and persistent (pink dots) heavy precipitation events. For Type 1 (Figure 7a), the stations with medium-long (blue dots) and long-duration (pink dots) heavy precipitation are mainly located along the Yangtze River, indicating that these areas are more prone to long-duration heavy precipitation than other regions. This is related to the path of the southwest vortex, which often moves eastward along the Yangtze River and disappears into the sea. Heavy precipitation of Type 2 (Figure 7b) is mainly distributed in the mountains of Northeastern Jiangxi and near Huangshan mountains. There are no stations where persistent heavy precipitation events of Type 1 and Type 2 with  $T \geq 6$  h ever occurred. This is probably due to the fact that frontal systems over the MLRYR basin tend to be mobile [44]. The rapid movement of a frontal system can easily cause short-duration heavy precipitation events with  $T \leq 3$  h. Although a quasi-stationary frontal system usually causes long-duration precipitation events, few of them meet the rain intensity of 5 mm/h for  $>4$  h. For Type 3 (Figure 7c), medium-long-duration precipitation usually falls in the western parts of Hubei and the transverse band-shape area in central Jiangxi. Yao Xiuping et al. (2022) [45] pointed out that 70% of the shear lines in the Jianghuai region would cause rainstorms, and warm shear line rainstorms contribute most to the rainfall of the shear-line rainstorms in the Jianghuai region; the bands of rainstorms caused by shear lines are consistent with the directions of the shear lines. For the Type 4 warm inverse trough (Figure 7d), medium-long-duration precipitation mainly occurs in the lower reaches of the Yangtze River, while other regions have mainly short-duration heavy precipitation. Sun et al. [46] found that rainstorm areas mainly appear at the top of warm inverse troughs usually on the southeast wind side, when warm and cold air interact with each other. For Type 5 (Figure 7e), medium-long-duration heavy precipitation mainly occurs in the areas exposed to the main body of the typhoon in the eastern part of the lower reaches of the Yangtze River as well as in Hunan and Western Hubei. The stations with long-duration precipitation over 6 h under Type 5

circulation are the majority and the most concentrated among the six synoptic circulation patterns. Type 6 (Figure 7f) easterly waves often cause medium- or long-duration heavy precipitation events with  $4\text{ h} \leq T \leq 5\text{ h}$  in Western Hubei, Jiangxi, and Southern Hunan. For the easterly wave-related precipitation, meso- and fine-scale surface wind convergence caused by the terrain is likely to occur in the mountainous areas of Southern Hunan, and the angle included between the orientation of mountain ranges and the coming direction of warm and humid airflow plays a significant role in the distribution of intense precipitation. The warm and humid flow in the boundary layer brought by an easterly wave trough tends to cause deep mesoscale vortices on the windward slope, thus significantly increasing the rainfall of tropical systems such as typhoons and easterly waves [47], and there are large mountain ranges in both of the two areas, which are the main causes for the extreme rainstorms.

### 3.4. Propagation Characteristics of Diurnal Variations of Heavy Precipitation

The MLRYR region roughly features a mountain-plain-mountain-plain topography with an east-west orientation, so the temporal variation of the MLRYR region roughly features a mountain-plain-mountain-plain topography with an east-west orientation, so the temporal variation of precipitation has a significant difference between the east and west of the region. Many studies showed that the peak diurnal variation of precipitation along the Yangtze River propagates from the Eastern Tibetan Plateau towards downstream [48,49], but few of them analyzed in detail the characteristics of peak diurnal variations of heavy precipitation under different synoptic circulation patterns and the impacts of these patterns on the propagation of heavy precipitation. Figure 5 shows the normalized time-longitude or time-latitude distribution of heavy precipitation under the effect of the six synoptic circulation patterns (note: the normalized method is the hourly precipitation  $\geq 20\text{ mm/h}$  divided by the 24 h total precipitation of the day). As a whole, the heavy precipitation centers are divided into a scattered mountainous region west of  $112^\circ\text{ E}$ , a transitional plain-like zone between  $112$  and  $114^\circ\text{ E}$ , and a patchy distribution east of  $114^\circ\text{ E}$  (Figure 8). After classification, the synoptic systems responsible for heavy precipitation in this region are distinct, which leads to different characteristics of heavy precipitation in distribution. The Type 1 (Figure 8a) heavy precipitation has double frequency peaks during 11:00–17:00 BT and 00:00–06:00 BT, respectively. Its duration of heavy precipitation is the longest among the six types. The central value of precipitation is located near  $111^\circ\text{ E}$  at 10:00 h and propagates eastward until it reaches near  $120^\circ$  at 13:00–16:00 h. The eastward propagation time of the entire system is about 6 h, and the central value of precipitation features an obvious eastward propagation. How do different synoptic circulation patterns affect propagation characteristics? Type 1 is mainly the result of the synergy effects among systems such as the southwestern vortex, subtropical high, and Meiyu front. The stable subtropical high periphery continues to deliver a strong local southward warm and humid flow to the middle and lower reaches of the Yangtze River. Systems such as southwest vortices or low-level jets are disturbed on the Meiyu front and move southward along with the North China high-pressure air to propagate the peak of heavy precipitation eastward together with the synoptic systems. Type 2 heavy precipitation events show double frequency peaks near  $27$ – $31^\circ\text{ N}$  (Meiyu area) during 10:00–16:00 and 02:00–07:00, respectively, and a single peak in non-Meiyu areas. Type 2 mainly features local oscillations rather than north-south propagation. Type 2 is often carried southward by northeastern cyclones with weak cold air and forms a frontal surface with the cyclones in the Jianghuai region, usually an east-west transverse shear. The synoptic system would stop causing persistent heavy precipitation, resulting in insignificant north-south propagation characteristics. The heavy precipitation center of Type 3 (Figure 8c) is mainly located in Jiangxi and Hunan regions to the south of  $28^\circ\text{ N}$ , and the peak frequency occurs during 11:00–21:00. Under this synoptic circulation pattern, cold high-pressure systems often appear in Northeast China. As the cold high-pressure system moves southward, the warm shear line also retreats southward, leading to the southward propagation of the precipitation center. Type 4 (Figure 8d) heavy

precipitation events dominated by easterly flows show a single frequency peak in 9:00–19:00. In the area to the south of  $28^{\circ}$ , it propagates mainly from south to north. In the area to the north of  $30^{\circ}$  N, it mainly propagates northward. Since Type 4 often occurs when the southwest vortex in the basin and the cyclone in North China are not active, the 850 hPa warm shear system, in conjunction with the development of a warm inverse trough on the ground, would trigger the formation of MCSs when the small cold air masses from North China move southward into the warm inverse trough. When the cold air is strong, after the warm inverse trough reaches near  $28^{\circ}$  N, it is dominated by southward movement. When the cold air is weak, the warm low-pressure system keeps developing and moving northward and can reach  $30^{\circ}$  N, showing a northward propagation characteristic. The centers of both Type 5 and Type 6 heavy precipitation events are localized without propagation characteristics. Type 5 (Figure 8e) is combined with the mid-latitude westerly trough through the typhoon body and mainly affects the lower reaches of the Yangtze River, as well as Western Hubei and Western Hunan, by causing extreme precipitation events. Due to the combination of easterly flows and terrain uplift, Type 6 (Figure 8f) often triggers local severe convective weather.

To sum up, influenced by the movement of different synoptic systems and the superposition of local thermodynamic circulations, the propagation characteristics of the heavy precipitation frequency over the MLRYR basin differ significantly. The central value of Type 1 (vortex/shear line) heavy precipitation propagates eastward from near  $111^{\circ}$  E, and the eastward propagation time of the entire system is about 6 h. Type 2 (frontal surface) heavy precipitation events show double frequency peaks near the Meiyu area and a single peak in non-Meiyu areas without significant north-south propagation characteristics. The heavy precipitation center of Type 3 (warm shear line) (Figure 5c) is mainly located in Jiangxi and Southern Hunan and propagates mainly southward. In the area to the south of  $28^{\circ}$  N, the center of Type 4 (warm inverse trough line) heavy precipitation events propagates mainly from north to south, while in the area to the north of  $30^{\circ}$  N, it mainly propagates northward. The centers of Type 5 (typhoon-westerly trough) and Type 6 (easterly wave) heavy precipitation events are localized without propagation characteristics.

### 3.5. Temporal Phase Differences of Maximum Precipitation Amount

According to Figure 2 above, the peaks and valleys of heavy precipitation in the four study regions appear alternately and can be roughly divided into four periods: 04:00–09:00 BT, 10:00–12:00 BT, 13:00–21:00 BT, and 22:00–03:00 BT. The daily peak precipitation time is defined as the time when the maximum precipitation occurs in 11 years at each station. Therefore, what are the differences in the temporal phase distribution of peak precipitation amounts under the six synoptic circulation patterns during the two peak phases of 04:00–09:00 and 13:00–21:00? As shown in Figure 6, the daily precipitation peaks at different stations are not consistent and are distributed in multiple phases, especially in phase 04:00–09:00. The phase stations are most dispersed during the early morning peak. The precipitation peaks for Type 1 (Figure 9a) and Type 2 (Figure 9b) events dominated by southwesterly flows in central and Western Hubei and Southern Jiangxi mainly occur during 13:00–21:00, while the peaks in other regions occur in multiple phases alternately. The peaks for Type 3 (Figure 9c) precipitation events mainly occur in the morning phase in Western Hunan, but in the afternoon phase in the lower reaches of the Yangtze River. This is probably due to the fact that the warm shear lines mainly move from west to east and from south to north under the guidance of monsoon flows [43]. For the synoptic patterns guided by the easterly flows, the peaks seldom occur in the morning phase and mainly occur in phase 13:00–21:00 (Figure 9d–f). The pronounced afternoon peak is apparently related to the increased local instability due to diurnal solar heating [33].

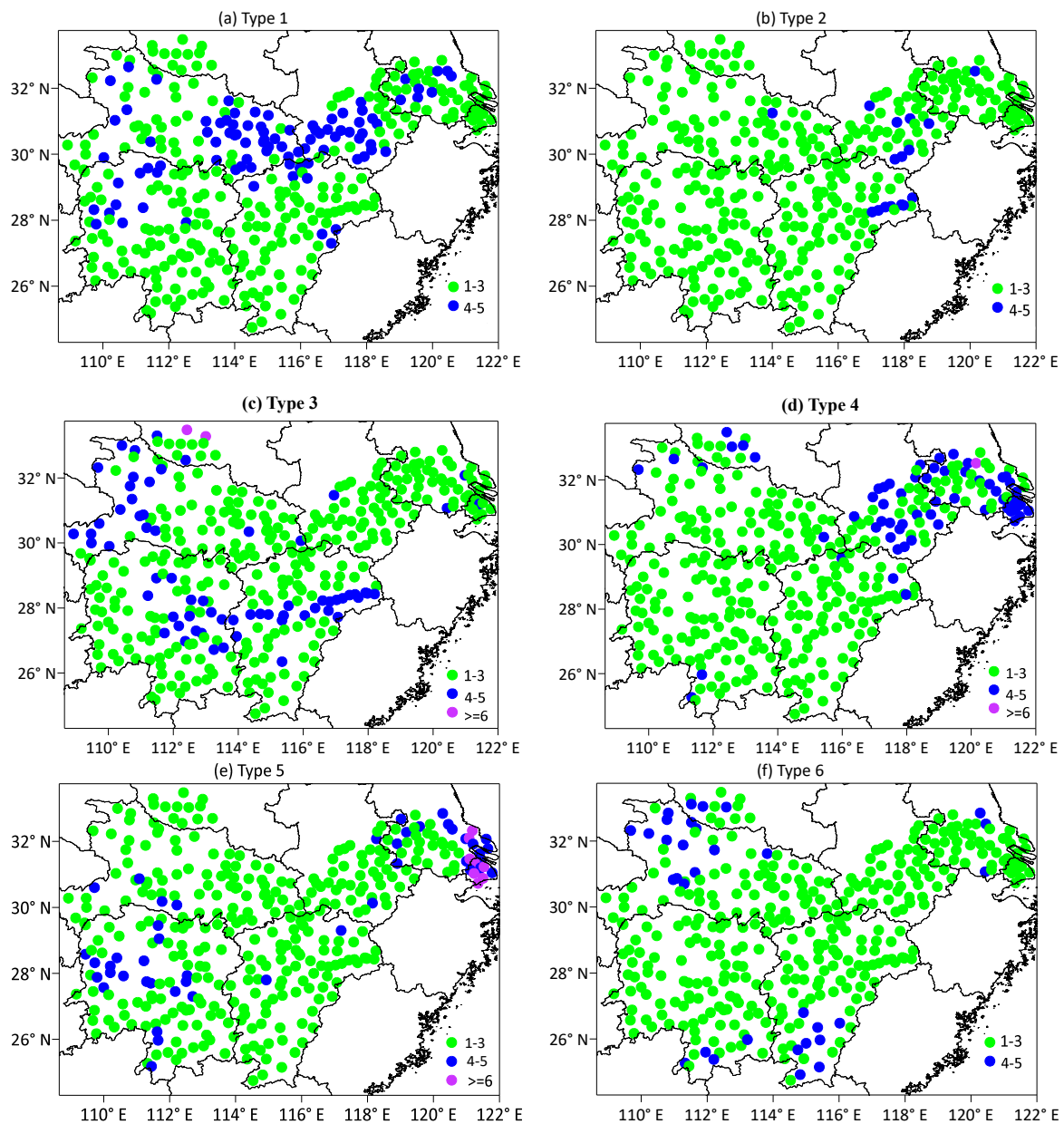


**Figure 7.** Distribution characteristics of the average duration of heavy precipitation under the 6 synoptic circulation patterns (green dots represent short-duration heavy precipitation  $\leq 3$  h, blue dots represent medium-to-long duration heavy precipitation for 4–5 h, and pink dots are long-duration heavy precipitation  $\geq 6$  h). (Computing method: For a certain weather circulation pattern, for a certain station, select the longest duration that meets the heavy precipitation conditions every day, mark it as the longest duration  $t(n)$  ( $n = 1, 2, 3 \dots N$ ,  $N$  is the number of days of a certain circulation pattern), and then divide it by the number of occurrences. Therefore, the result is the average of the longest duration of all cases of a certain weather circulation pattern at each station. (a–f) figures represents six weather circulation patterns, as shown in Figure 2.

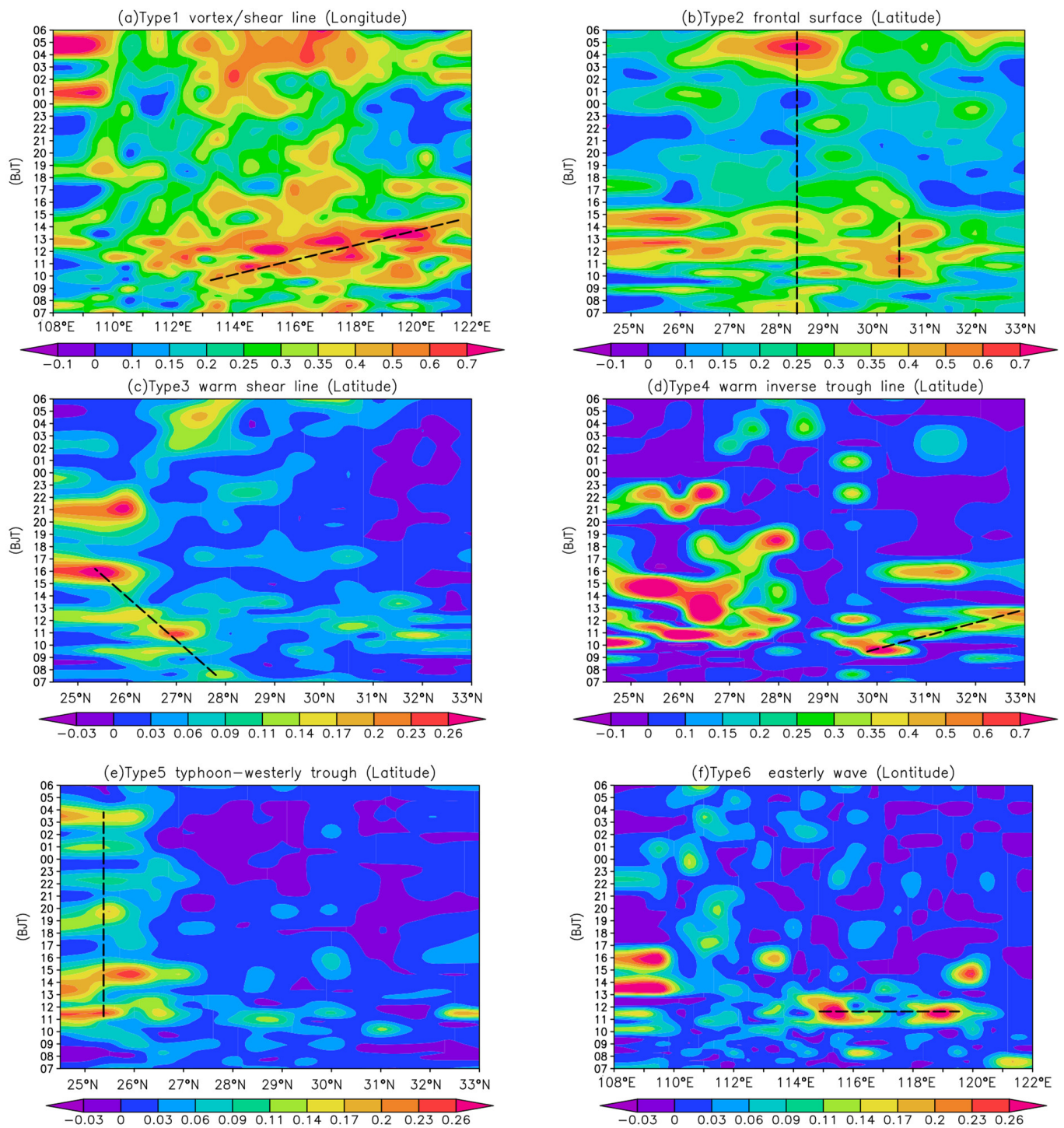


**Figure 8.** Time–longitude propagation and distribution characteristics of normalized heavy precipitation of the 6 synoptic circulation patterns (normalized by dividing the hourly precipitation  $\geq 20$  mm/h by the total 24 h precipitation of the day). (a–f) figures represents six weather circulation patterns, as shown in Figure 2. The dashed lines represents the propagation direction of normalized heavy precipitation.

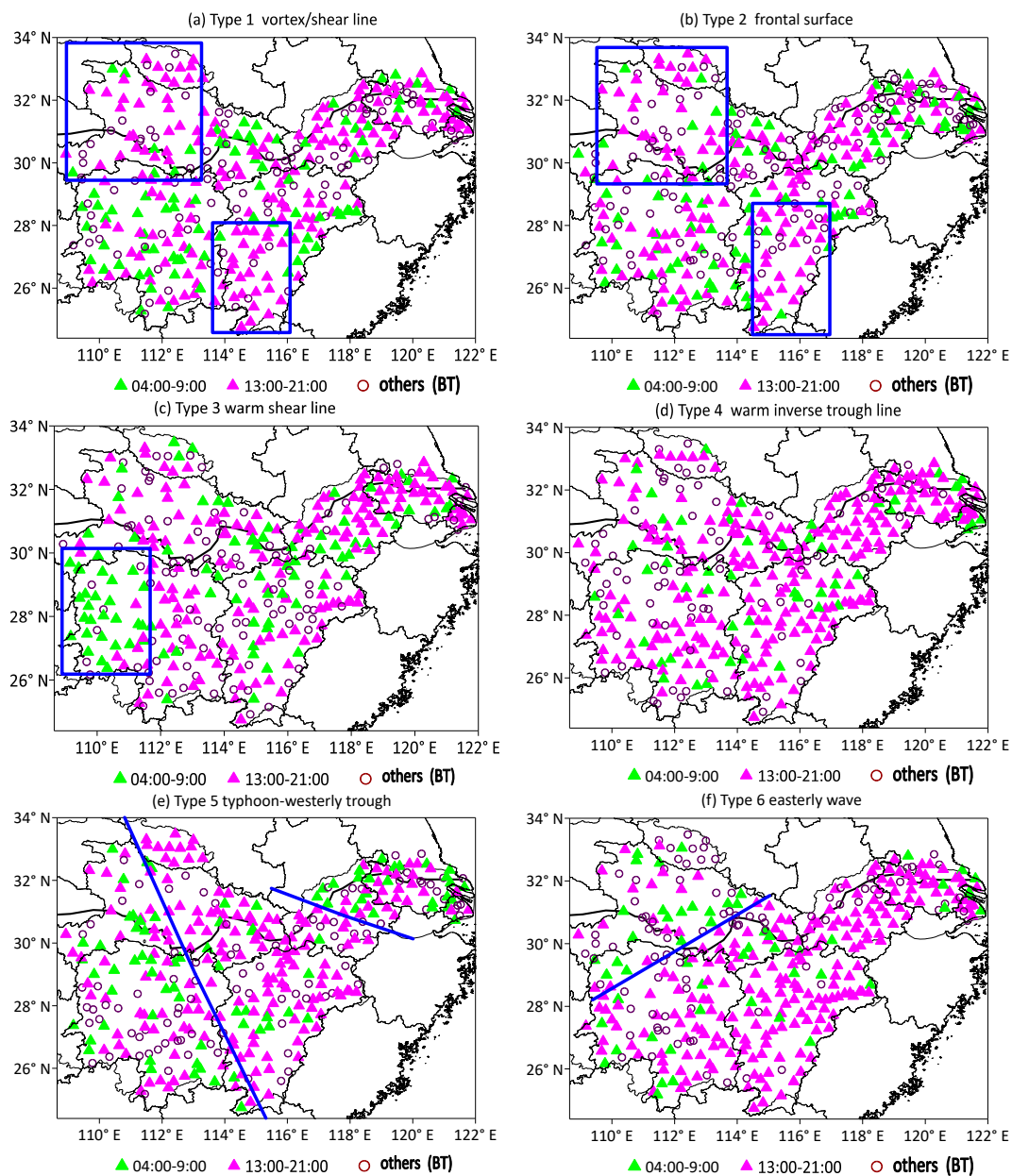


**Figure 9.** Time phase distribution of peak precipitation in two heavy precipitation periods in 04:00–09:00 BT, 13:00–21:00 BT, and others under the six synoptic circulation patterns. (a–f) figures represents six weather circulation patterns, as shown in Figure 2. (The box line and the straight line are the prominent areas of peak precipitation in the morning or afternoon, or the boundary between the two).

#### 4. Interconfiguration of Multilayer Systems of Six Synoptic Circulation Patterns

The positions of the South Asian High (SAH) and Northwest Pacific subtropical high (WNPSH) play an important role in the formation of heavy summer precipitation events in the MLRYR [3]. To study how different synoptic circulation patterns affect heavy precipitation in the MLRYR, the configurations of multilayer synoptic systems under different synoptic circulation patterns are further given in Figure 7. Under the prevailing southwest monsoon pattern (Type 1–3, Figure 10a–c), the 200 hPa South Asian high is significantly located eastward to the climatological position with its eastern end extending near 115° E, and the 500 hPa subtropical high is located near the climatological position with its western end extending near 120° E. The two high-pressure systems attract each other. A water vapor channel is formed between the peripheries of the two high-pressure

systems, and the vapor flux from the South China Sea and the Bay of Bengal is carried by the southerly flow to the middle and lower reaches of the Yangtze River. The water vapor of Type 1 and Type 2 mainly originates from the western part of the South China Sea, while that of Type 3 mainly originates from the eastern part of the South China Sea. According to the synthetic diagnosis results, there are significant updrafts and cape values at 700 hPa in rainstorm areas (figure omitted), but only the cape of Type 1 passed the significance test. It indicates that for Type 1, dynamical lifting and thermal lifting play balanced roles, while for the other two types, dynamical lifting plays a key role. Under the easterly flow pattern (Type 4–6, Figure 10d–f), the SAH and WNPSH are shifted northward compared to their climatological positions, significantly retreating westward or eastward compared with the prevailing southwest monsoon pattern.

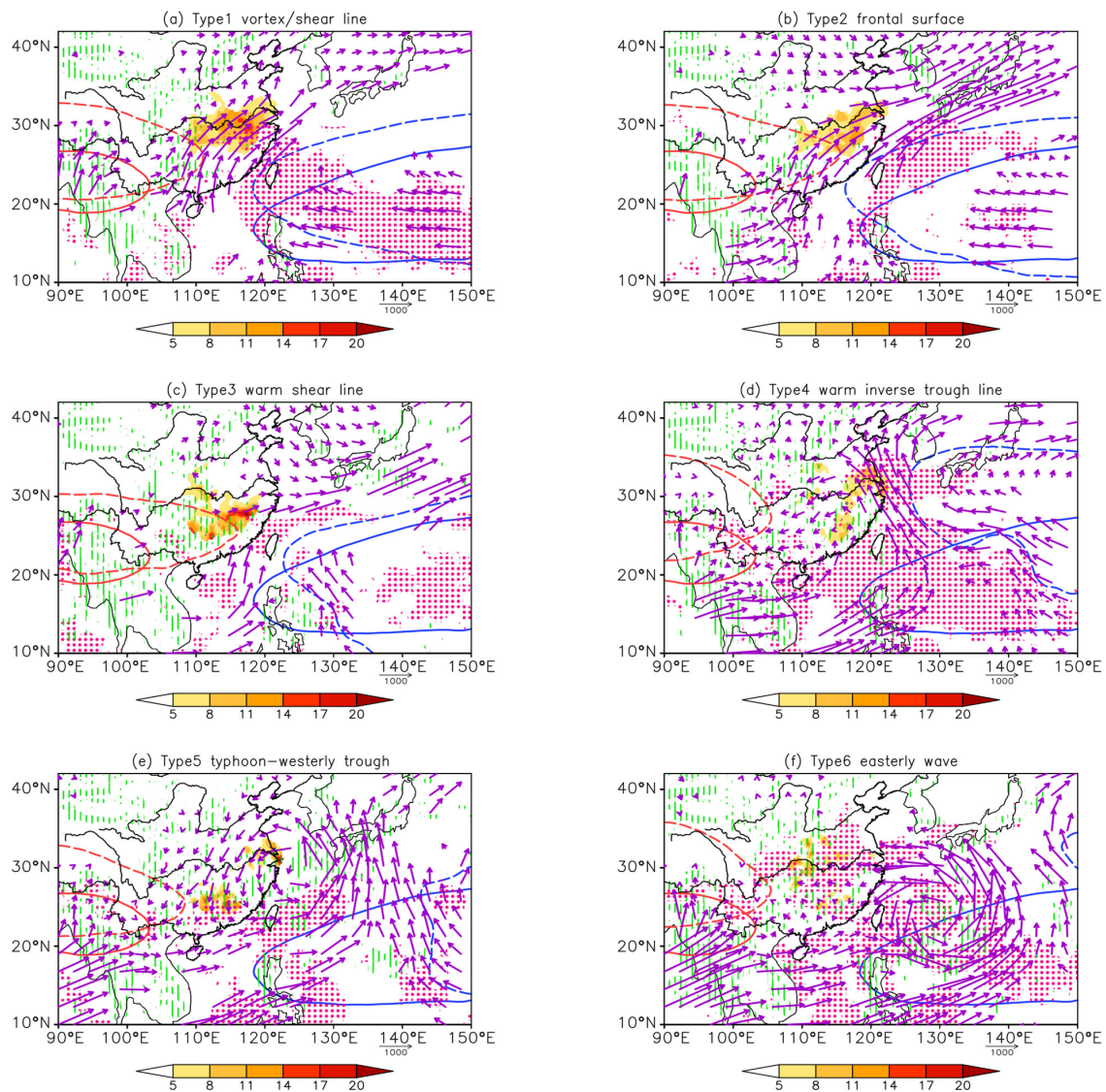


**Figure 10.** Configuration of South Asian High (SAH) and Northwest Pacific subtropical high (WNPSH) under each synoptic pattern. Short dashed red (blue) lines refer to SAH (WNPSH), and solid red (blue) lines refer to their summer climatological positions in SAH (WNPSH). Vectors indicate the vertically integrated water vapor flux (1000–300 hPa). Green vertical lines indicate the ascent speed is more than 1 cm/s at 850 hPa. Red-dotted areas indicate the vertically integrated CAPE. All significant levels are 0.05, as tested by Student’s *t*-test. Shaded values are the occurrence probability of extreme precipitation. (a–f) figures represents six weather circulation patterns, as shown in Figure 2.

The two high-pressure systems repel each other. The water vapor flux mainly originates from the East China Sea. According to synthetic diagnosis results, Type 4 and Type 5 correspond poorly to the cape value (figure omitted), indicating that the precipitation events are mainly caused by dynamical lifting. However, in the rainstorm area, most of the w values and cape values pass the significance test with a confidence level of 0.1, indicating that precipitation is attributed to dynamical lifting, while heavy precipitation must be accompanied by favorable cape values.

### 5. Long-Term Trends of Six Synoptic Circulation Patterns

Statistics of the linear trends of the stations with a daily precipitation exceeding 50 mm under each synoptic type over the MLRYR basin show that the number of rainstorm stations for Type 2 (frontal surface) or Type 3 (warm shear line) dominated by the prevailing southwest monsoon (Figure 11a) presents an increasing trend in the past 10 years, while that for Type 1 (vortex/shear line) shows a slight increasing trend, which is somehow related to the recovered East Asian summer monsoon [50]. The number of rainstorm stations for the easterly flow (Figure 11b) for Type 4 (warm inverse trough line) or Type 6 (easterly wave) shows a decreasing trend, especially that for Type 4, which shows a significant decreasing trend, while that for Type 5 (typhoon-westerly trough) shows a slight increasing trend, which may be related to the increased typhoons over the northwest Pacific [51–53].

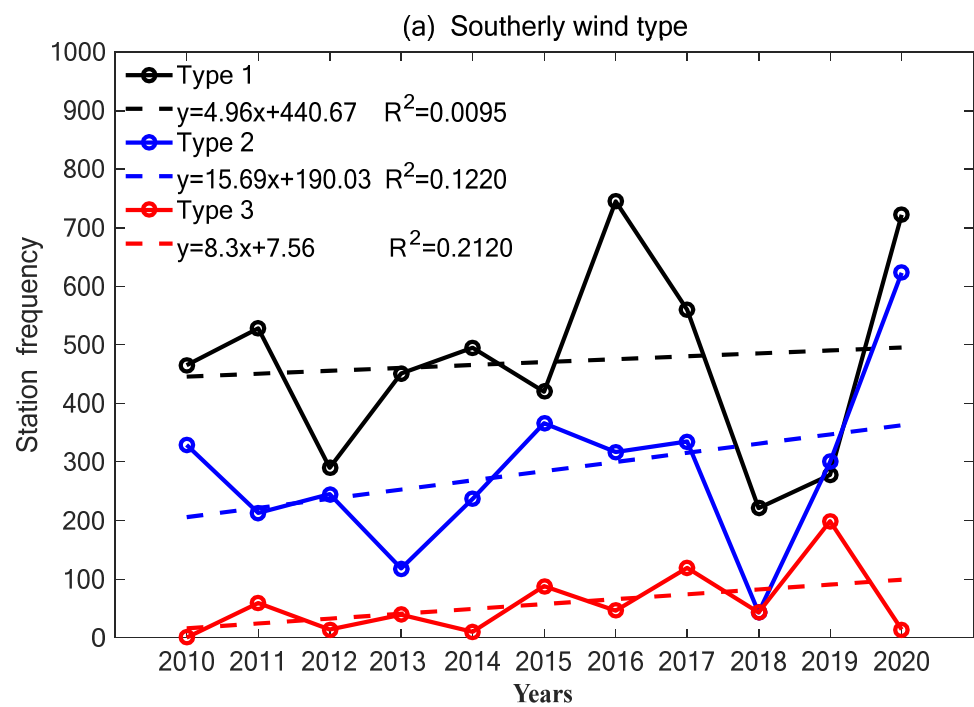
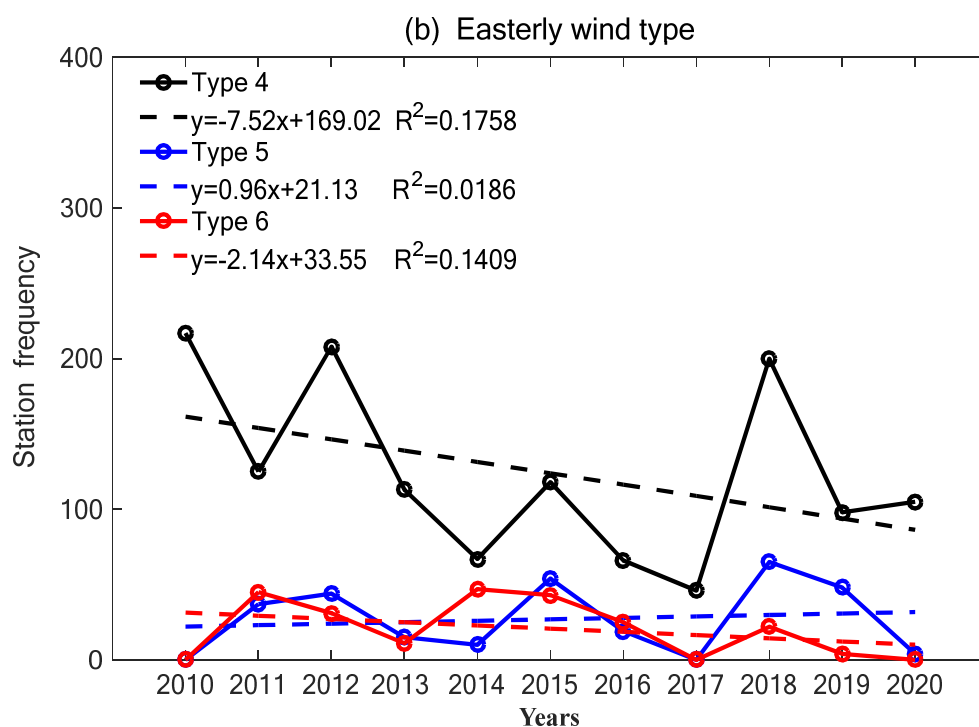


Figure 11. Cont.



**Figure 11.** Temporal variations of synoptic patterns associated with the station frequency of rainstorm days over MLRYR basin. Type1, Type2 and Type3 dominated by the prevailing southwest monsoon (a), Type4, Type5 and Type6 dominated by the easterly flow (b). (Solid circle lines show the frequency of the six patterns, and dotted lines show linear trend of the frequency with the significant level of 0.05 tested by *t*-test.).

## 6. Summary and Discussion

Based on hourly precipitation data after quality control, the characteristics of rainstorm during June–August ( $\geq 50$  mm/d) at 367 stations over the MLRYR basin over 2010–2020 have been studied. The daily average 850 hPa geopotential height fields are classified into six synoptic circulation patterns using the PCT method. We studied the configurations of different synoptic circulation patterns, their long-term trends, and their impacts on diurnal variations of heavy precipitation. It is not only conducive to understanding the different circulation backgrounds, daily variation characteristics, and rainstorm mechanisms of heavy rainfall in this area. Moreover, it is of great significance for studying the distribution, intensity, and onset time of floods caused by different weather circulation patterns, such as whole basin floods or local floods, providing references for forecasting precipitation, as well as flood prevention and control. The main conclusions are as follows:

The synoptic circulation patterns causing rainstorms over the MLRYR basin are mainly Type 1 (vortex/shear line), Type 2 (frontal surface), and Type 3 (warm shear line) dominated by the prevailing southwest monsoon, and Type 4 (warm inverse trough line), Type 5 (typhoon-westerly trough), and Type 6 (easterly wave) dominated by the easterly flow. Under the prevailing southwest monsoon, the 200 hPa SAH is significantly located eastward of the climatological position, and the 500 hPa WNPSH is located north of the climatological position. The southerly flow between the two high-pressure systems carries the vapor from the South China Sea and the Bay of Bengal to the middle and lower reaches of the Yangtze River. For Type 1, dynamical lifting and thermal lifting play balanced roles, while for the other two types, dynamical lifting plays a key role. From the perspective of the start time of heavy precipitation, the persistent and short-duration heavy precipitation events caused by Type 1, Type 2, and Type 3 show double peaks. The persistent ones show one primary and one secondary peak, and the short-duration ones show balanced double peaks. Heavy precipitation caused by Type 1 patterns is mostly persistent, and heavy precipitation events

start at night or in the morning. Heavy precipitation occurring under Type 2 and Type 3 patterns can be persistent heavy precipitation events or short-duration convective heavy precipitation events. Statistics of rainstorm stations over the past 10 years show that the number of rainstorm stations for Type 2 or Type 3 shows an increasing trend, while that for Type 1 shows a slight increasing trend, which is somehow related to the recovered East Asian summer monsoon.

Under the easterly flow pattern, the SAH and WNPSH are located near the climatological position, significantly retreating westward or eastward compared with high-pressure systems dominated by the southwesterly monsoon. The water vapor comes mainly from the East China Sea area. Type 5 and Type 6 are mainly affected by dynamical lifting, which can trigger heavy rainfalls, while heavy precipitation events with rainstorm intensity must be accompanied by favorable cape values. Heavy precipitation events of these types show a single peak frequency. Among them, the heavy precipitation events of Type 5 and Type 6 are mostly short-duration heavy precipitation events in the afternoon. Therefore, the peak diurnal variation of short-duration heavy precipitation events is related to both the afternoon solar radiation and the synoptic circulation pattern. The number of rainstorm stations for Type 4 or Type 6 shows a decreasing trend, especially that for Type 4, which shows a significant decreasing trend, while that for Type 5 shows a slight increasing trend, which may be related to the increased typhoons over the northwest Pacific.

The monsoon climate and complex terrains in East Asia have a significant impact on the occurrence of heavy precipitation events in the MLRYR in summer. Many issues regarding the impacts of different synoptic circulation patterns on the diurnal variations and mechanisms of precipitation and the interactions between multiscale weather systems are still to be solved.

The mechanism of the influence of synoptic circulation patterns on the diurnal variation of precipitation has not been analyzed enough in this paper. What causes multiscale weather systems to occur at different times of the day and lead to different durations of precipitation? What is the relationship between the diurnal variation of precipitation and SST, low-level wind speed, and water vapor transport? This remains to be further investigated.

**Author Contributions:** Conceptualization, H.Q. and C.L.; methodology, C.L., T.P. and H.Q.; software, H.Q. and C.L.; validation, C.C. and X.Z.; formal analysis, X.Z. and H.Q.; data curation, C.L. and Y.X.; writing—original draft preparation, H.Q. and C.L.; writing—review and editing, H.Q., Z.Y. and W.C.; supervision, C.L. and T.P.; project administration, C.L., T.S. and C.C.; funding acquisition, C.L., C.C. and H.Q. All authors have read and agreed to the published version of the manuscript.

**Funding:** This research is jointly supported by the Project of Yangtze River Basin Meteorological Opening Fund (CJLY2022Y06), Natural Science Foundation of Hubei Province (Joint Fund) (2022CFD129), Natural Science Foundation of Hubei Province (2022CFB025), Hubei Meteorological Science and Technology Development Fund of China (2020Z03, 2022Y06, 2022Y26, 2022Y05), the Project of Hubei Key Laboratory of Water System Science for Sponge City Construction (Wuhan University) (2021-07), the Special Program for Innovative Development of China Meteorological Administration (CXFZ22J08, CXFZ2022J019) and Basic Research Fund of WHIHR (202304).

**Institutional Review Board Statement:** Not applicable.

**Informed Consent Statement:** Not applicable.

**Data Availability Statement:** Please contact email qxynl@163.com for data.

**Acknowledgments:** The authors are very grateful to Dong Xi Quan, Deng Yi, Chen Gui Xing, Zhang Ling and Wang Jun Chao for their valuable suggestions.

**Conflicts of Interest:** The authors declare no conflict of interest.

## References

- Rao, X.N.; Zhao, K.; Chen, X.C.; Huang, A.N.; Xue, M.; Zhang, Q.H.; Wang, M.J.M. Influence of synoptic pattern and low-level wind speed on intensity and diurnal variations of orographic convection in summer over Pearl River Delta, South China. *J. Geophys. Res. Atmos.* **2019**, *2019*, JD030384. [\[CrossRef\]](#)
- Yin, S.Q.; Chen, D.L.; Xie, Y. Diurnal variations of precipitation during the warm season over China. *Int. J. Climatol.* **2009**, *29*, 1154–1170. [\[CrossRef\]](#)
- Tang, Y.; Huang, A.N.; Wu, P.L.; Huang, D.Q.; Xue, D.K.; Wu, Y. Drivers of summer extreme precipitation events over East China. *Geophys. Res. Lett.* **2021**, *48*, e2021GL093670. [\[CrossRef\]](#)
- Trenberth, K.E.; Dai, A.; Rasmussen, R.M.; Parsons, D.B. The changing character of precipitation. *Bull. Am. Meteorol. Soc.* **2003**, *84*, 1205–1217. [\[CrossRef\]](#)
- Zhai, P.M.; Zhang, X.B.; Wan, H.; Pan, X.H. Trends on total precipitation and frequency of daily precipitation extremes over China. *J. Clim.* **2005**, *18*, 1096–1108. [\[CrossRef\]](#)
- Yu, R.C.; Xu, Y.P.; Zhou, T.J.; Li, J. Relation between rainfall duration and diurnal variation in the warm season precipitation over central eastern China. *Geophys. Res. Lett.* **2007**, *34*, L13703. [\[CrossRef\]](#)
- He, H.Z.; Zhang, F.Q. Diurnal variations of warm-season precipitation over North China. *Mon. Weather Rev.* **2010**, *138*, 1017–1025. [\[CrossRef\]](#)
- Xu, W.X.; Zipser, E.J.; Liu, C.T. Rainfall characteristics and convective properties of Mei-Yu precipitation systems over South China, Taiwan, and the South China Sea. Part I: TRMM observations. *Mon. Weather Rev.* **2009**, *137*, 4261–4275. [\[CrossRef\]](#)
- Bañares, E.N.; Narisma, G.T.T.; Simpas, J.B.B.; Cruz, F.T.; Lorenzo, G.R.H.; Cambaliza, M.O.L.; Coronel, R.C. Seasonal and diurnal variations of observed convective rain events in Metro Manila, Philippines. *Atmos. Res.* **2021**, *258*, 105646. [\[CrossRef\]](#)
- Zhuo, H.; Zhao, P.; Zhou, T.J. Diurnal cycle of summer rainfall in Shandong of eastern China. *Int. J. Climatol.* **2014**, *34*, 742–750. [\[CrossRef\]](#)
- Liu, C.; Wang, D.Y.; Zheng, L.L. Characteristics of the diurnal variations flood period precipitation in Anhui during the last 30 years. *Torrential Rain Disaster* **2017**, *36*, 53–59. (In Chinese) [\[CrossRef\]](#)
- Zhu, L.M.; Liu, J.Z.; Zhu, A.X.; Sheng, M.L.; Duan, Z. Spatial distribution of diurnal rainfall variation in summer over China. *J. Hydrol.* **2018**, *19*, 667–678. [\[CrossRef\]](#)
- Huang, H.L.; Wang, C.C.; Chen, G.T.J.; Carbone, R.E. The role of diurnal solenoidal circulation on propagating rainfall episodes near the eastern Tibetan Plateau. *Mon. Weather Rev.* **2010**, *138*, 2975–2989. [\[CrossRef\]](#)
- Sun, J.H.; Zhang, F.Q. Impacts of mountain-plains solenoid on diurnal variations of rainfalls along the Mei-Yu front over the east China plains. *Mon. Weather Rev.* **2012**, *140*, 379–397. [\[CrossRef\]](#)
- Soderholm, B.; Ronalds, B.; Kirshbaum, D.J. The evolution of convective storms initiated by an isolated mountain ridge. *Mon. Weather Rev.* **2014**, *142*, 1430–1451. [\[CrossRef\]](#)
- Wu, Y.; Huang, A.; Huang, D.; Chen, F.; Yang, B.; Zhou, Y.; Fang, D.; Zhang, L. Diurnal variations of summer precipitation over the regions east to Tibetan Plateau. *Clim. Dyn.* **2018**, *51*, 4287–4307. [\[CrossRef\]](#)
- Li, M.X.; Zhang, Q.H.; Zhang, F.Q. Hail Day Frequency Trends and Associated Atmospheric Circulation Patterns over China during 1960–2012. *J. Clim.* **2016**, *29*, 7027–7044. [\[CrossRef\]](#)
- Yu, R.; Li, J. Hourly rainfall changes in response to surface air temperature over eastern contiguous China. *J. Clim.* **2012**, *25*, 6851–6861. [\[CrossRef\]](#)
- Li, J.; Yu, R.C.; Yuan, W.H.; Chen, H.M. Changes in duration-related characteristics of late-summer precipitation over Eastern China in the past 40 years. *J. Clim.* **2011**, *24*, 5683–5690. [\[CrossRef\]](#)
- Yuan, W.H.; Yu, R.C.; Zhang, M.H.; Lin, W.Y.; Chen, H.M.; Li, J. Regimes of diurnal variation of summer rainfall over subtropical East Asia. *J. Clim.* **2012**, *25*, 3307–3320. [\[CrossRef\]](#)
- Jiang, Z.N.; Zhang, D.L.; Xia, R.D.; Qian, T.T. Diurnal variations of presummer rainfall over Southern China. *J. Clim.* **2017**, *30*, 755–773. [\[CrossRef\]](#)
- Kottayil, A.; Satheesan, K.; Viju, O.J.; Antony, R. Diurnal variation of deep convective clouds over Indian monsoon region and its association with rainfall. *Atmos. Res.* **2021**, *255*, 105540. [\[CrossRef\]](#)
- Schumacher, R.S.; Johnson, R.H. Organization and environmental properties of extreme-rain-producing mesoscale convective systems. *Mon. Weather Rev.* **2005**, *133*, 961–976. [\[CrossRef\]](#)
- Schumacher, R.S.; Clark, A.J.; Xue, M.; Kong, F.Y. Factors influencing the development and maintenance of nocturnal heavy-rain-producing convective systems in a storm-scale ensemble. *Mon. Weather Rev.* **2013**, *141*, 2778–2801. [\[CrossRef\]](#)
- Kerns, B.W.J.; Chen, Y.L.; Chang, M.Y. The diurnal cycle of winds, rain, and clouds over Taiwan during the Mei-Yu, summer, and autumn rainfall regimes. *Mon. Weather Rev.* **2010**, *138*, 497–516. [\[CrossRef\]](#)
- Leppert, K.D.; Cecil, D.J. Tropical cyclone diurnal cycle as observed by TRMM. *Mon. Weather Rev.* **2016**, *144*, 2793–2808. [\[CrossRef\]](#)
- Wang, C.C.; Chien, F.C.; Paul, S.; Lee, D.I.; Chuang, P.Y. An evaluation of WRF rainfall forecasts in Taiwan during three Mei-Yu seasons from 2008 to 2010. *Weather Forecast.* **2017**, *32*, 1329–1351. [\[CrossRef\]](#)
- Liu, W.R.; Cook, K.H.; Vizy, E.K. The role of mesoscale convective systems in the diurnal cycle of rainfall and its seasonality over sub-Saharan Northern Africa. *Clim. Dyn.* **2019**, *52*, 729–745. [\[CrossRef\]](#)
- Nesbitt, S.W.; Zipser, E.J. The diurnal cycle of rainfall and convective intensity according to three years of TRMM measurements. *J. Clim.* **2003**, *16*, 1456–1475. [\[CrossRef\]](#)

30. Chang, C.P.; Hou, S.C.; Kuo, H.C.; Chen, G.T.J. The development of an intense East Asian summer monsoon disturbance with strong vertical coupling. *Mon. Weather Rev.* **1998**, *126*, 2692–2712. [[CrossRef](#)]
31. Ding, Y.H.; Chan, J.C.L. The East Asian summer monsoon: An overview. *Meteorol. Atmos. Phys.* **2005**, *89*, 117–142. [[CrossRef](#)]
32. Wang, Y.; Zhou, L. Observed trends in extreme precipitation events in China during 1961–2001 and the associated changes in large-scale circulation. *Geophys. Res. Lett.* **2005**, *32*, L09707. [[CrossRef](#)]
33. Luo, Y.L.; Wu, M.W.; Ren, F.M.; Li, J.; Wong, W.K. Synoptic situations of extreme hourly precipitation over China. *J. Clim.* **2016**, *29*, 8703–8719. [[CrossRef](#)]
34. Stryhal, J.; Huth, R. Classifications of winter Euro-Atlantic circulation patterns: An intercomparison of five atmospheric reanalyses. *J. Clim.* **2017**, *30*, 7847–7861. [[CrossRef](#)]
35. Carlaw, L.B.; Cohen, A.E.; Rogers, J.W. Synoptic and mesoscale environment of convection during the north American Monsoon across central and southern Arizona. *Weather Forecast.* **2017**, *32*, 361–375. [[CrossRef](#)]
36. Zhang, J.G.; Wang, J.; Wu, T.; Zhou, J.L.; Zhong, M.; Wang, S.S.; Huang, X.Y.; Li, S.; Han, F.; Wang, C. Weather system types of extreme precipitation in the middle reaches of the Yangtze River. *Torrential Rain Disasters* **2018**, *37*, 14–23. (In Chinese) [[CrossRef](#)]
37. Dzung, N.L.; Yamada, T.J. Using weather pattern recognition to classify and predict summertime heavy rainfall occurrence over the upper Nan River basin, northwestern Thailand. *Weather Forecast.* **2019**, *34*, 345–360. [[CrossRef](#)]
38. Liu, R.X.; Sun, J.H.; Chen, B.F. Selection and classification of warm-sector heavy rainfall events over South China. *Chin. J. Atmos. Sci.* **2019**, *43*, 119–130. (In Chinese) [[CrossRef](#)]
39. Huth, R.; Beck, C.; Philipp, A.; Demuzere, M.; Ustrnul, Z.; Cahynová, M.; Kyselý, J.; Tveito, O.E. Classifications of atmospheric circulation patterns. *Ann. N. Y. Acad. Sci.* **2008**, *1146*, 105–152. [[CrossRef](#)]
40. Philipp, A.; Bartholy, J.; Beck, C.; Erpicum, M.; Esteban, P.; Fettweis, X.; Huth, R.; James, P.; Jourdain, S.; Kreienkamp, F.; et al. Cost733cat-database of weather and circulation type classifications. *Phys. Chem. Earth* **2010**, *35*, 360–373. [[CrossRef](#)]
41. Demuzere, M.; Kassomenos, P.; Philipp, A. The COST733 circulation type classification software: An example for surface ozone concentrations in Central Europe. *Theor. Appl. Climatol.* **2011**, *105*, 143–166. [[CrossRef](#)]
42. Hersbach, H.; Bell, B.; Berrisford, P.; Hirahara, S.; Horányi, A.; Muñoz-Sabater, J.; Nicolas, J.; Peubey, C.; Radu, R.; Schepers, D.; et al. The ERA5 Global Reanalysis. *Q. J. R. Meteorol. Soc.* **2020**, *146*, 1999–2049. [[CrossRef](#)]
43. Chen, H.M.; Yu, R.C.; Li, J.; Yuan, W.H.; Zhou, T.J. Why nocturnal long duration rainfall presents an eastward-delayed diurnal phase of rainfall down the Yangtze River valley. *J. Clim.* **2010**, *23*, 905–917. [[CrossRef](#)]
44. Zhao, Y.; Deng, L.; Li, Z.W.; Wang, Y.J. Quantitative Attribution of Vertical Motion Responsible for Summer Heavy Rainfall Over North China. *J. Geophys. Res. Atmos.* **2022**, *127*, e2021JD035765. [[CrossRef](#)]
45. Yao, X.P.; Zhang, H.H.; Ma, J.L.; Shi, D.W.; Wang, W.J.; Wang, G.C. Characteristics of newly formed mesoscale convective systems during the abnormal precipitation over the Yangtze River basin from June to July, 2020. *Atmos. Sci. Lett.* **2022**, *23*, e1114. [[CrossRef](#)]
46. Sun, X.C. Study on the formation mechanism of rainstorms associated with surface inverted troughs. *J. Mar.* **2018**, *38*, 39–46. (In Chinese) [[CrossRef](#)]
47. Hu, Z.J.; Li, L.; Huang, X.Y.; He, B.W.; Ye, R.X. Analysis of mechanism of topographic influence and meso-scale convective characteristics of an extremely severe rainfall affected by typical easterly wave. *J. Arid. Meteorol.* **2022**, *40*, 73–83. [[CrossRef](#)]
48. Zhang, H.; Zhai, P.M. Temporal and spatial characteristics of extreme hourly precipitation over eastern China in the warm season. *Adv. Atmos. Sci.* **2011**, *28*, 1177–1183. [[CrossRef](#)]
49. Hu, Y.; Deng, Y.; Zhou, Z.M.; Cui, C.G.; Dong, X.Q. A statistical and dynamical characterization of large-scale circulation patterns associated with summer extreme precipitation over the middle reaches of Yangtze River. *Clim. Dyn.* **2019**, *52*, 6213–6228. [[CrossRef](#)]
50. Zhao, G.J.; Huang, G.; Wu, R.G.; Tao, W.C.; Gong, H.N.; Qu, X.; Hu, K. A new upper-level circulation index for the east asian summer monsoon variability. *J. Clim.* **2015**, *28*, 9977–9996. [[CrossRef](#)]
51. Kossin, J.P.; Knapp, K.R.; Olander, T.L.; Velden, C.S. Global increase in major tropical cyclone exceedance probability over the past four decades. *Proc. Natl. Acad. Sci. USA* **2020**, *117*, 11975–11980. [[CrossRef](#)] [[PubMed](#)]
52. Qiu, W.; Ren, F.; Wu, L.; Chen, L.; Ding, C. Characteristics of tropical cyclone extreme precipitation and its preliminary causes in Southeast China. *Meteorol. Atmos. Phys.* **2019**, *131*, 613–626. [[CrossRef](#)]
53. Wang, C.; Yoon, S.K.; Chen, J.; Chen, H.; Xiong, L.H.; Kim, J.S. Statistical prediction of typhoon-induced total accumulated rainfall in the Western North Pacific using typhoon track similarity indices. *Atmos. Res.* **2023**, *288*, 106724. [[CrossRef](#)]

**Disclaimer/Publisher’s Note:** The statements, opinions and data contained in all publications are solely those of the individual author(s) and contributor(s) and not of MDPI and/or the editor(s). MDPI and/or the editor(s) disclaim responsibility for any injury to people or property resulting from any ideas, methods, instructions or products referred to in the content.